Journal of Materials Chemistry B

ROYAL SOCIETY OF CHEMISTRY

PAPER

View Article Online
View Journal | View Issue



Cite this: J. Mater. Chem. B, 2026, 14, 4173

# Galactose-decorated lipid nanoparticle-mediated delivery of a selective NLRP3 inhibitor attenuates hepatic inflammation in metabolic dysfunction-associated steatotic liver disease

Chunyan Niu, †*[a] Wen Gao,†[a] Mei Tan,†[a] Yue Chen,†[a] Yongqiang Shi,[a] Yan Geng,[b] Huayi Tao,[a] Zhenjiang Xu,[a] Tingting Zhang[a] and Jinming Yang*[c]

Received 13th November 2025,
Accepted 28th February 2026

DOI: 10.1039/d5tb02289d

rsc.li/materials-b

Metabolic dysfunction-associated steatotic liver disease (MASLD) is a metabolic stress-induced hepatic injury closely associated with insulin resistance and genetic predisposition, affecting about 25% of the global population and becoming the leading cause of chronic liver disease. Therapeutic interventions targeting the regulation of inflammation-related pathways have shown potential for significant improvements in MASLD treatment. Herein, we developed galactose-decorated lipid nanoparticles for selective NLRP3 inhibitor targeted liver delivery (MCC950@Gal-LNPs). The galactose modification endowed the LNPs with liver-targeting ability *via* asialoglycoprotein receptor (ASGPR)-based hepatocellular uptake. The MCC950-loaded formulation effectively reduced the expression of inflammatory regulators and cytokines associated with the NF-κB/NLRP3-related signaling pathway. The Gal-LNPs improved MCC950 accumulation in the liver compared to non-targeted formulations and effectively reduced inflammatory signal activation *in vivo*. Moreover, MCC950 treatment significantly improved fibrosis by reducing the fibrotic area and normalizing tissue morphology. Therefore, MCC950@Gal-LNPs significantly reduces the inflammatory microenvironment, and MCC950, as a novel NLRP3 inhibitor, appears to be an attractive assay for the effective treatment of NASLD.



## Introduction

Non-alcoholic fatty liver disease (NAFLD) is a metabolic stress-induced hepatic injury closely associated with insulin resistance and genetic predisposition.[1,2] Currently affecting 25.24% of the global population, NAFLD has emerged as the primary contributor to chronic liver diseases, hepatic fibrosis, and hepatocellular carcinoma.[3] Within the NAFLD spectrum, approximately 20-25% of patients develop non-alcoholic steatohepatitis (NASH), a progressive subtype with significant oncogenic potential.[4] This advanced stage substantially increases risks of progression to hepatic fibrosis, cirrhosis, end-stage liver disease, hepatocellular carcinoma (HCC), and liver-related mortality while concurrently elevating susceptibility to obesity, diabetes, and cardiovascular disorders through extrahepatic metabolic dysregulation.[5] The clinical challenge stems from NAFLD/NASH's typically asymptomatic progression and late-stage identification,[6] particularly since advanced fibrosis accelerates disease progression. NASH represents a critical transition point from benign fatty liver to severe hepatic pathology. Early detection of NASH with significant fibrosis and timely intervention could effectively prevent, delay, or reverse disease progression, thereby substantially reducing NAFLD-related cirrhosis, end-stage liver disease, and HCC-related morbidity/mortality.[7] Despite growing recognition of NAFLD's clinical significance, diagnostic limitations persist. The complex pathogenesis has hindered the establishment of definitive diagnostic criteria or specific biomarkers globally. Notably, no pharmacological agents have received approval from either the European Medicines Agency or the US Food and Drug Administration (FDA) for NAFLD treatment.[7,8] However, recent years have witnessed substantial advancements in elucidating disease mechanisms, driving intensified research efforts toward targeted therapeutic development.

Recent research indicates that NAFLD, analogous to type 2 diabetes, constitutes a systemic metabolic disorder.[9] In 2020, experts proposed renaming it "metabolic-associated fatty liver disease (MAFLD)" to emphasize the critical role of metabolic

[a] Department of Gastroenterology, Nanjing Lishui People's Hospital, Zhongda Hospital Lishui Branch, Southeast University, Nanjing, 211200, China. E-mail: nchy69@163.com
[b] Department of Endocrinology, Nanjing Lishui People's Hospital, Zhongda Hospital Lishui Branch, Southeast University, Nanjing, 211200, China
[c] Endoscopy Center, Nanjing Lishui People's Hospital, Zhongda Hospital Lishui Branch, Southeast University, Nanjing, 211200, China. E-mail: 2389121017@qq.com
† These authors contributed equally to this work.

dysregulation.[10] In 2023, they officially replaced MAFLD with the new concept of metabolic dysfunction-associated steatotic liver disease (MASLD). The emerging ''multiple parallel hit'' theory posits that MASLD pathogenesis involves concurrent interactions between multiple factors and genetic susceptibility, leading to hepatic inflammation, hepatocyte apoptosis, hepatic stellate cell activation, fibrogenesis, and disease progression.[11] The chronic low-grade inflammatory microenvironment serves as the central mechanism underlying hepatocyte injury, providing crucial pathophysiological foundations for MASLD development. Notably, the NLRP3 inflammasome functions as both an inflammatory cascade regulator and a key driver of hepatic inflammation, particularly in metabolic dysfunction-associated steatohepatitis (MASH)-related fibrosis. It activates pro-inflammatory pathways and promotes disease progression from MASLD to MASH, ultimately contributing to advanced fibrosis and hepatocellular carcinoma.[12–14]

Current experimental evidence demonstrates elevated NLRP3 inflammasome activity in NASH animal and cellular models. Therapeutic interventions targeting NLRP3 have significantly improved metabolic parameters, hepatocyte protection, and fibrosis attenuation.[15] These approaches also ameliorate age-related metabolic dysfunction and hepatic inflammation in murine models.[16,17] NLRP3 inflammasome is expressed in both liver cells and HSCs.[18] It can sense various signals such as free fatty acids (FFAs), lipopolysaccharides, TNF-α, cholesterol crystals, DAMPs, and PAMPs and participate in inflammation amplification, HSC activation, liver fibrosis, and the development of cirrhosis. Activating the LRP3 inflammasome is a prerequisite for the development of MASLD fibrosis,[19] which in turn induces HSC activation and the occurrence and development of liver fibrosis. The NLRP3/caspae-1/IL-1β pathway activation and induced cell pyroptosis are important pathways leading to liver inflammation.[19,20] MCC950, as a selective inhibitor of NLRP3, has shown that it can improve the pathology and fibrosis of MAFLD in obese diabetic mice, which could normalize the NLRP3/caspae-1/IL-1β pathway and reduce the expression of AST and ALT,[21–23] providing a new direction and strong research basis for the development of specific targeted drug therapy for NASH.

In recent years, emerging delivery materials (*e.g.*, polymeric nanoparticles, stimuli-responsive carriers, and biomimetic systems) have improved drug solubility, systemic circulation, and intracellular bioavailability by rationally tuning the particle size, surface properties, and formulation stability.[24–26] Among these platforms, lipid nanoparticles (LNPs) offer distinct advantages owing to their modular composition, scalable manufacturing, broad payload compatibility, and capacity to protect therapeutics while facilitating cellular uptake and intracellular delivery. Moreover, galactose (Gal) functionalization can leverage asialoglycoprotein receptor (ASGPR)-mediated endocytosis, which is highly active in hepatocytes, to enhance liver-targeted accumulation and hepatocellular internalization, thereby improving therapeutic efficacy and reducing off-target tissue exposure.

This research designed liver cell-targeted lipid nanoparticles (LNPs) for MCC950 effective delivery. The drug-loaded LNPs (MCC950@Gal-LNPs) were formulated by nanoprecipitation assay. The galactose modification endowed the liver-targeting ability of liposomes. The hepatocyte-targeted delivery of MCC950 using galactose-decorated LNPs enhances hepatic delivery/uptake and thereby inhibits NLRP3 inflammasome activation, leading to reduced inflammatory signaling and attenuation of inflammation-associated liver fibrosis in MASLD-relevant models.

## Results and discussion

### MCC950@Gal-LNP formula optimization

Signal factor experiments were used to optimize the formulation of MCC950@Gal-LNPs. The amounts of formulation components, such as DODAP, cholesterol, and DSPE-PEG2000-Gal, the hydration buffer pH, and the drug/lipid ratio were optimized. Firstly, HEPES buffer with different pH values in the formulation was evaluated (Fig. 1A). The drug-loaded LNPs prepared at pH 7.4 buffer exhibited a size of 78.3 ± 1.5 nm with the lowest PDI value, but the formulation prepared in buffer with different pH values exhibited an increment of PDI without significant differences in the size. The zeta potential data suggested that the formulation prepared at pH 7.4 has a lower zeta potential (Fig. 1F). For component optimization, we evaluated the effects of the amounts of cholesterol, DSPE-PEG2000-Gal, and DODAP on the particle size and zeta potential of LNPs (Fig. 1B–D and F). Cholesterol mainly works as the lipid membrane fluidity regulator in lipid-based formulations. Suitable cholesterol content could improve the membrane rigidity and stability of particles. The formulation prepared with cholesterol accounts for 15% of total lipids, showing the lowest particle size and negative zeta potential but a higher PDI value. In comparison, the LNPs prepared with DODAP account for 20% of the total lipids and have similar results. The DODAP, as a positive lipid, improves the ability to interact with cell membranes and cellular uptake. An increased DODAP content in LNPs did not significantly affect the particle size but significantly increases the zeta potential, making it more positively charged, which might lead to rapid ERS elimination. Therefore, 20% was chosen as the optimized content of DODAP. With the increase in the amount of DSPE-PEG2000-Gal, the particle size of LNPs slightly decreased. After comprehensive consideration, we selected the prescription of LNPs with 15% of cholesterol, 10% of DSPE-PEG2000-Gal, 20% of DODAP, and 55% of DOPE and then prepared them with HEPES buffer at pH 7.4. Then, the drug loading was evaluated, and data showed that the drug/lipid ratio reached 40%, exhibiting a suitable particle size and acceptable PDI (Fig. 1E).

Based on the optimized prescription, we formulated drug-loaded LNPs, and their physicochemical properties were evaluated. The optimized MCC950@Gal-LNPs exhibited a uniform particle size at 102.6 ± 1.8 nm with a PDI of 0.295 ± 0.102. The zeta potential of MCC950@Gal-LNPs was −14.6 ± 3.5 mV. The MCC950 loading (DL) reached 26.8 ± 1.3%, suggesting LNPs as a potential drug delivery system with high drug loading capacity.

 

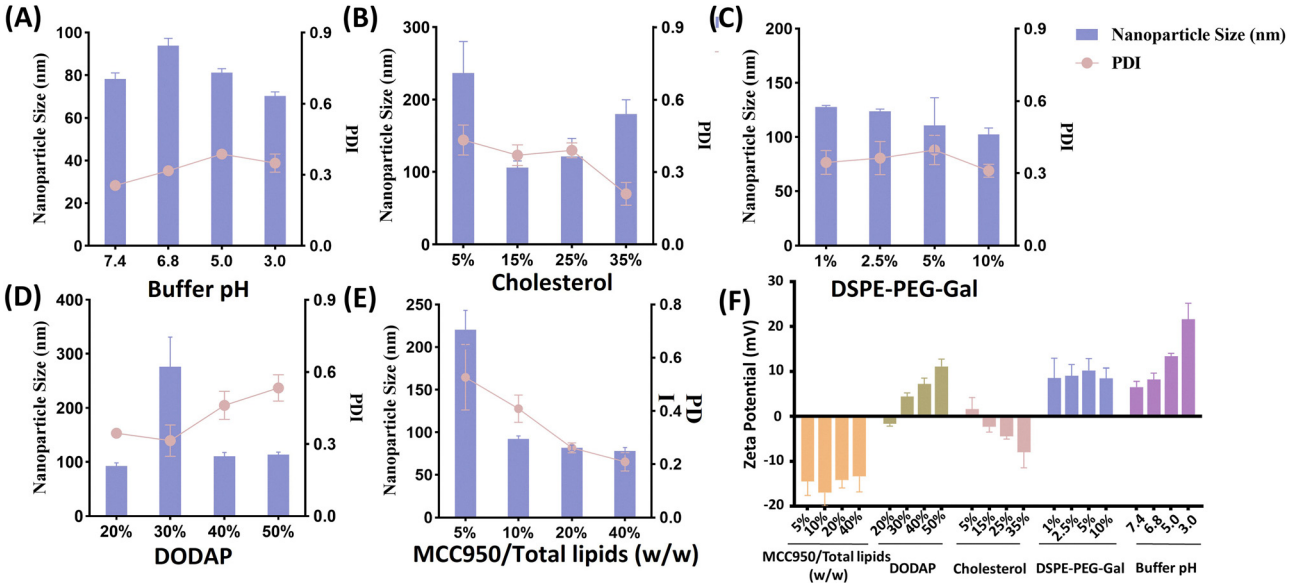


Fig. 1 Formula optimization of MCC950@Gal-LNPs by signal factor experiment. Effects of (A) HEPES buffer pH value, (B) contents of cholesterol, (C) contents of DSPE-PEG2000-Gal, (D) contents of DODAP, and (E) MCC950/total lipid mass ratio on the particle size and PDI of MCC950@Gal-LNPs. (F) The effects of the above factors on the zeta potential of MCC950@Gal-LNPs. All data is represented as mean ± SD ($n$ = 3).

### Stability investigation

We further evaluated the stability of the optimized MCC950@Gal-LNPs formulations and used the MCC950@LNPs as a control. Both formulations were stored at 37 °C, and their particle size and distribution were measured. As shown in Fig. 2, the particle size of MCC950@LNPs could keep stabilization at first 12 hours but exhibited a particle size increment after 24 hours of storage at 37 °C. For the MCC950@Gal-LNPs, no significant particle size difference was observed after 24 h storage, with PDI slightly increased but still less than 0.3. The data suggested the formulation could remain stable at body temperature during systemic circulation after administration for at least 24 hours and exhibited its potential to extend body circulation.

### Anti-inflammatory effects of MCC950@Gal-LNPs in MASLD cell model

To evaluate the anti-inflammatory effects of MCC950@LNPs *in vivo*, we first established the MASLD AML-12 cell (hepatocytes) model. The cells were co-incubated with fatty acid molding fluid at different concentrations for 24 hours. After incubation, we fixed cells with paraformaldehyde and stained cells with the Modified Oil Red O staining kit to evaluate the MASLD induction. As shown in Fig. 3A, only a small number of oil droplets were stained red in the negative control group, while the fatty acid model fluid incubation led to a large amount of red staining area in cells with deeper color, suggesting the MASLD cell model establishment was successful. As the concentration increment of the model fluid, the induced cell contains more oil droplets with a deeper red color but does not affect cell morphology and proliferation state. Therefore, we chose the high-concentration fatty acid model fluid to establish MASLD cells.

The effects of MCC950 on MASLD treatment efficacy were evaluated by incubating LPS first and then treating it with MCC950. NF-κB, as the key inflammatory regulator, controls a lot of pro-inflammatory cytokine synthesis and release. Here, we evaluated the expression of NF-κB and TNF-α in mRNA and protein levels (Fig. 3B–F). Compared to the model group, cells treated with MCC950 could effectively reduce the expression of NF-κB and downstream TNF-α. Between them, MCC950@Gal-LNPs exhibited the lowest NF-κB in mRNA compared to other treatment groups, which we speculated was due to the Gal-based cellular uptake improvement, suggesting the effectively reduced intracellular inflammation. However, at the protein level, the intracellular TNF-α protein expression was no different between the free MCC950 and MCC950-loaded formulation groups, possibly due to the TNF-α released from the cell.

To evaluate the MASLD prevention, cells were incubated with MCC950 first and then induced inflammation by incubating with LPS. As shown in Fig. 3B–F, the free MCC950 and MCC950-loaded formulations all exhibited effects in reducing inflammation. In comparison, the formulation groups exhibited a stronger

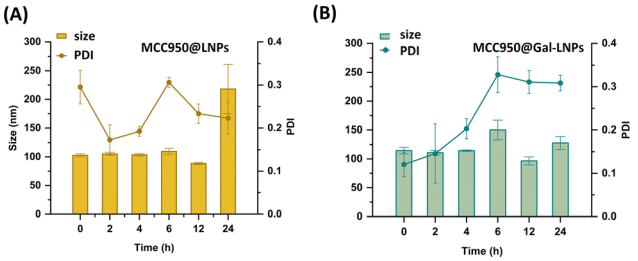


Fig. 2 Stability of MCC950@LNPs and MCC950@Gal-LNPs. The particle size and PDI values of (A) MCC950@LNPs and (B) MCC950@Gal-LNPs after incubation at 37 °C for 24 hours. All data are represented as mean ± SD ($n$ = 3).

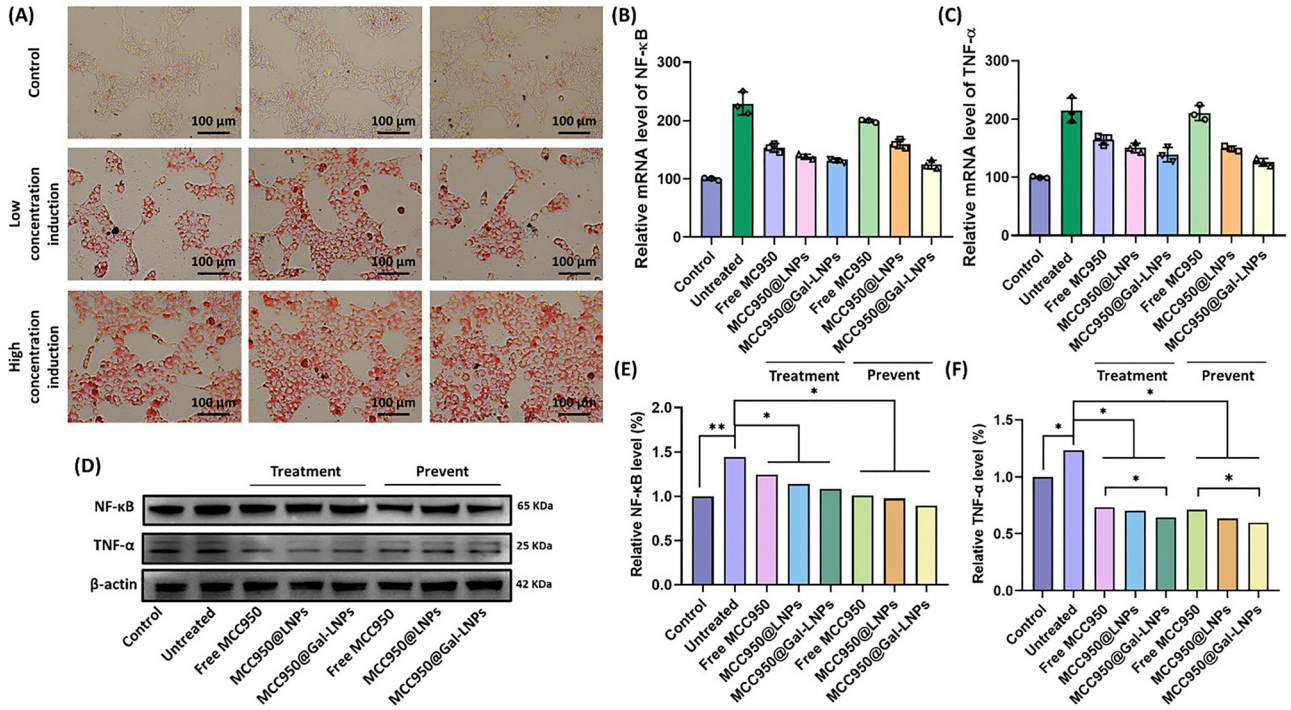


Fig. 3 Anti-inflammatory effects of MCC950@Gal-LNPs in MASLD cells. (A) Oil red O staining in AML-12 cells after fatty acid induction, fluid incubation and observed under an inverted microscope. Expression of NF-κB and TNF-α in (B) and (C) mRNA level and (D) protein level after incubation with different MCC950 formulations. (E) and (F) The expression of protein level quantity using Image J software. All data is represented as mean ± SD ($n$ = 3).

ability to inhibit inflammation, which might be due to the prolonged drug release of the formulation intracellularly. However, we found the protein level of TNF-α shows no significant difference. TNF-α is a rapidly induced and secreted cytokine. After inflammatory stimulation, TNF-α is often synthesized and secreted quickly; therefore, intracellular/lysate TNF-α levels measured by western blot at a single endpoint may not reflect differences in total production or secretion. The expression of NF-κB and TNF-α in mRNA and protein levels was reduced after treatment with MCC950-loaded formulation, suggesting MCC950 could also prevent the MASLD progression.

### Biodistribution of Gal-LNPs *in vivo*

To improve the therapeutic efficiency and reduce toxicity, we designed galactose-modified LNPs for improving MCC950 target delivery to hepatocytes. To evaluate the biodistribution of MCC950@Gal-LNPs *in vivo*, we first established the MASLD mouse model using BALB/c mice. Mice were injected intraperitoneally with 20% carbon tetrachloride olive oil solution (w/w) every two days, lasting for four weeks at a dose of 0.1 mL.

Then, the biodistribution of drug-loaded formulations was evaluated in MASLD mice. Mice were administered with free DiD, DiD-loaded LNPs, and Gal-LNPs by i.v. injection (2 mg kg$^{-1}$ of DiD) and fluorescence intensity in mice were monitored by the IVIS instrument at different time intervals. The body fluorescence is shown in Fig. 4A. Unlike the free dye group, the DiD-loaded LNPs group and Gal-LNPs group exhibited a significant liver accumulation, and the Gal-modified formulation exhibited stronger fluorescence signals in the liver compared to normal LNP groups, suggesting the Gal-modification improved liver accumulation (Fig. 4B). The DiD signals in blood were also evaluated, and only free Dye groups exhibited signals 48 hours after administration, indicating that the LNP system effectively reduces undesirable distribution and exhibits the potential to reduce toxicity (Fig. 4C). The biodistribution data suggested that formulated MCC950 effectively improved the *in vivo* transportation, prolonged retention, and exhibited potential in liver targeted delivery and hepatocytes precision treatment.

When discussing the biodistribution results, it should be noted that hepatocyte uptake of Gal-LNPs is primarily mediated by ASGPR, and the level and activity of this receptor may change with disease progression. In the fibrosis model applied in this work, MCC950@Gal-LNPs showed higher liver accumulation, which is consistent with ASGPR-associated delivery under our experimental conditions. In late-stage fibrosis or cirrhosis, alterations in hepatocyte mass and liver microstructure may be accompanied by reduced or uneven ASGPR expression, which could affect both targeting efficiency and the distribution of nanoparticles among liver cell types. Therefore, evaluating ASGPR expression across different disease stages will be important to further validate and extend the targeting performance of this system in advanced disease settings and in human MASLD/MASH.

### Anti-inflammatory efficiency of MCC950@Gal-LNPs *in vivo*

The MASLD mice were established and treated with different formulations (Free MCC950, MCC950@LNPs, and MCC950@Gal-LNPs, equivalent to 2 mg kg$^{-1}$ of MCC950) every three days for a total of five times. The mice's body weight was monitored during

 

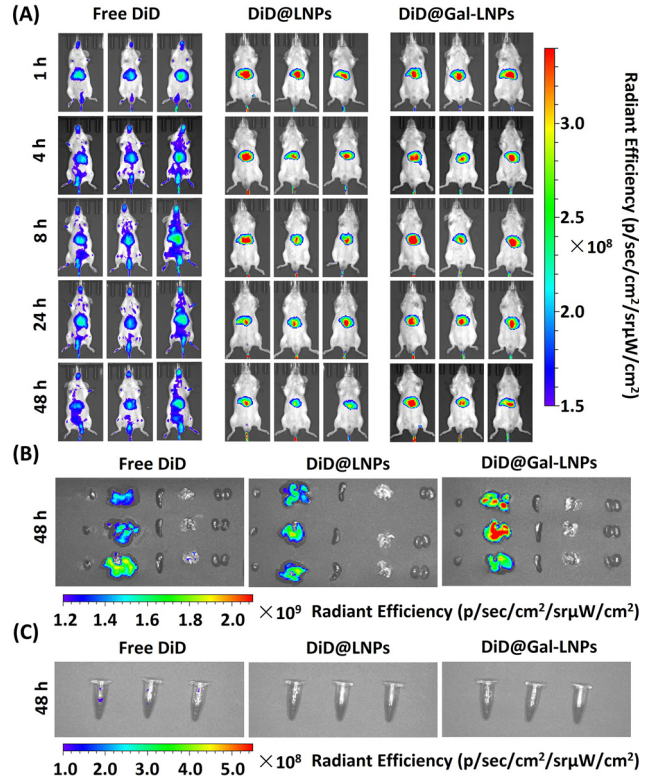


Fig. 4 *In vivo* biodistribution of DiD@Gal-LNPs. (A) The representative IVIS images of MASLD mice after administration with different formulations at different time intervals. The representative IVIS images of (B) isolated major organs and (C) blood from MASLD mice after administration of various formulations for 48 hours. All data is represented as mean ± SD ($n$ = 3).

the investigation, and, as shown in Fig. 5A, there was no obvious increase or decrease in body weight of mice from any research groups, indicating no significant acute toxicity *in vivo*. To evaluate the anti-inflammatory effects, livers from different treatment mouse groups were isolated, and several fibrosis regulators were analyzed using the western blot assay. α-SMA, as an activation maker of the hepatic stellate cell (HSC), usually increases with the severity of liver fibrosis; TGF-β is the cytokine released from inflammatory cells with the ability to promote activation of the downstream Samds signaling pathway and induce tissue fibrosis. As shown in Fig. 5B–D, expression of α-SMA and TGF-β was significantly increased in the model group than the control groups, suggesting the $CCl_4$ modeling successfully induced liver fibrosis in mice. The mice treated with MCC950 in different groups exhibited decreased protein expression, indicating MCC950 has the ability to combat liver fibrosis. Between them, the mouse liver from the MCC@Gal-LNP groups showed the lowest fibrosis-related protein expression, suggesting Gal-modification improves LNP accumulation in the liver.

Moreover, we further measured the inflammation-related genes such as IL-6 and NLRP3. As shown in Fig. 5E and F, MASLD model groups have increased expression of IL-6 and NLRP3 mRNA compared to the control group, confirming that severe inflammation was successfully induced in mice from the model group. After being treated with MCC950, the mRNA of IL-6 and NLRP3 was reduced in the control groups, confirming the anti-inflammation of MCC950. Similarly, MCC950@Gal-LNPs exhibited the lowest IL-6 and NLRP3 gene expression, suggesting the advantages in regulating inflammation.

MCC950 functions as a selective inhibitor of NLRP3 inflammasome activation. By restraining NLRP3-driven inflammasome assembly/activation, MCC950 is expected to reduce caspase-1 activation and thereby limit the processing and release of the mature pro-inflammatory cytokines IL-1β and IL-18. Given that these cytokines amplify hepatic inflammatory cascades and can promote fibrogenic signaling, attenuating the NLRP3–caspase-1 axis provides a plausible mechanistic bridge between our formulation-mediated delivery enhancement and the observed improvements in inflammatory readouts and fibrosis-associated markers. Importantly, our data support suppression of the NLRP3-related inflammatory pathway, while a full delineation of downstream network effects will require additional time-course and pathway-level analyses.

### Liver function evaluation after MCC950@Gal-LNPs treatment *in vivo*

The liver function of MASLD mice after MCC950 treatment was also investigated. The ALT and AST level in blood was measured after different formulation treatments. As shown in Fig. 6, AST and ALT levels in model groups significantly increased compared to the control group, indicating the MASLD mice have liver damage. After being treated with MCC950, MCC950@LNPs, or MCC950@Gal-LNPs, the ALT and AST levels significantly reduced from the model group, while no difference between several treatment groups, suggesting MCC950 exhibited potential against liver damage.

Moreover, the liver from mice was fixed and stained by H&E. As shown in Fig. 7A, the liver from the model group exhibited balloon-like cell shape exchange, cytoplasmic atrophy, and loose cell arrangement, suggesting liver damage formation. After treatment, liver tissue was partially repaired with cell morphology recovery and cellular nucleus normalization, especially in the MCC950@Gal-LNPs group, indicating their potential against liver damage. Additionally, we further analyzed fibrosis in liver tissue *via* the Masson's trichrome staining. As shown in Fig. 7B, there was no significant collagen deposition observed in the mouse liver from the control group, while severe collagen fiber deposition (thick and numerous blue collagen fibers) was observed in the MASLD model mice group, with unevenly distributed and patchy fibrin deposition areas, indicating a deeper degree of liver fibrosis. MCC950 treatment significantly improved fibrosis by reducing fibrotic area and normalizing tissue morphology. The MCC950@Gal-LNPs exhibited the most anti-fibrosis efficacy, indicating the targeted formulation as a potential way to utilize the therapeutic effect of MCC950.

## Experimental

### Materials

MCC950 was purchased from Aladdin Biochemical Technology Co., Ltd (Shanghai, CN). DSPE-PEG2000, cholesterol, and DOPE

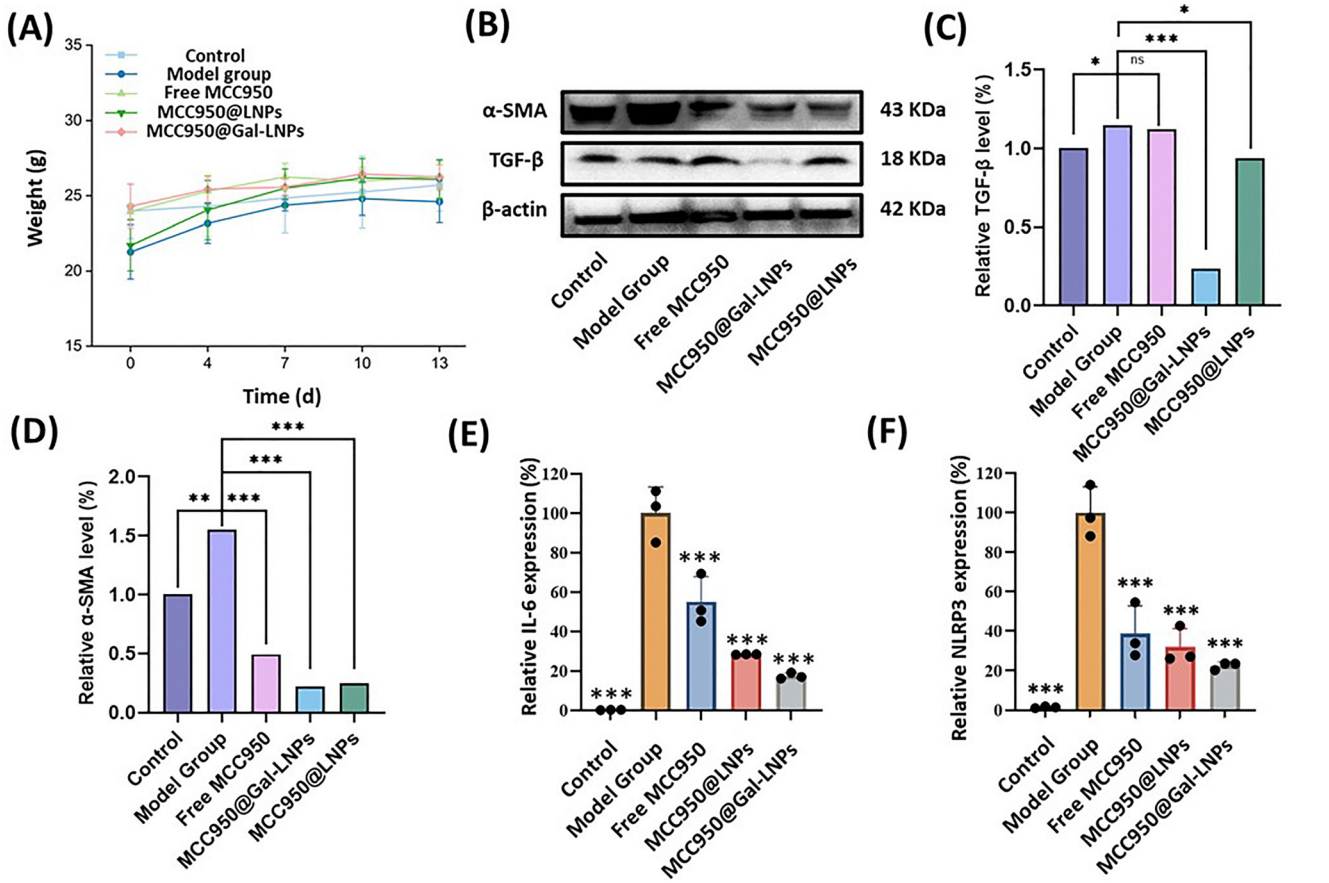


Fig. 5 Anti-inflammatory efficiency of MCC950@Gal-LNPs *in vivo*. (A) The body weight difference of mice after treatment. (B) The protein expression of α-SMA and TGF-β in different treatment groups. Quantification of western blot bands for (C) TGF-β and (D) α-SMA expression using ImageJ software in the liver from MASLD mice after treatment. The mRNA expression of (E) IL-6 and (F) NLRP3 in different treatment groups. All data is represented as mean ± SD ($n$ = 3).

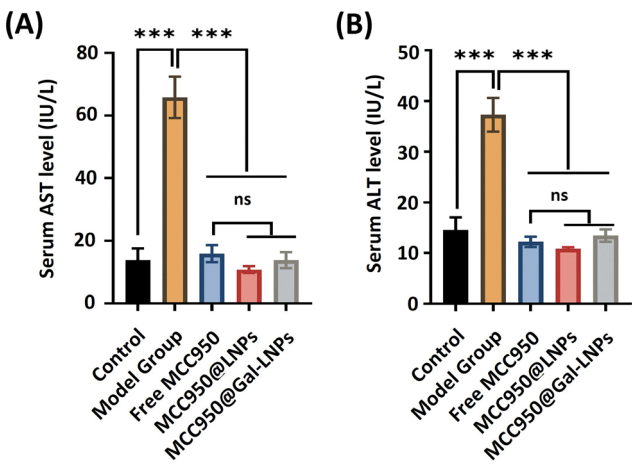


Fig. 6 MCC950 against liver damage in MASLD mice. The (A) AST and (B) ALT levels in mouse serum after treatment with MCC950 in various formulations. All data is represented as mean ± SD ($n$ = 3).

were purchased from AVT Pharmaceutical Tech Co., Ltd (Shanghai, CN). DSPE-PEG2000-Gal was purchased from Guangzhou Weihua Biological Technology Co., Ltd (Guangzhou, CN). DODAP was purchased from Bide Pharmatech Co., Ltd (Shanghai, CN). Lipopolysaccharide (LPS) was purchased from Sigma-Aldrich Corporation (Shanghai, CN). BCA kit, ALT kit, AST kit, TRIzol® reagent, and Taq Pro Universal SYBR qPCR Master Mix kit were purchased from Vazyme Biotech Co., Ltd (Nanjing, CN). RNAeasy™ RNA Isolation Kit was purchased from Beyotime Biotech Co., Ltd (Shanghai, CN). The primary antibodies (NF-κB, TNF-α, TGF-β, α-SMA, and β-actin) were purchased from Santa Cruz Biotechnology (Shanghai), Inc. (Shanghai, CN). 5X all-in-one RT MasterMix was purchased from Applied Biological Materials, Inc. (Vancouver, CA). The q-PCR primers of IL-6, NLRP3, and β-actin were purchased from General Biosystems (Anhui) Co., Ltd (Chuzhou, CN). All other chemicals and reagents were purchased from Shanghai Macklin Biochemical Co., Ltd (Shanghai, CN).

### Mammalian cells and animals

AML-12 cells were purchased from Nanjing Keygen Biotech. Co., Ltd (Nanjing, China). AML-12 cells were cultured in the DMEM/F12 medium, containing 10% fetal bovine serum (FBS) and 1% penicillin/streptomycin, and maintained in a 37 °C incubator supplemented with 5% $CO_2$ for further use.

 

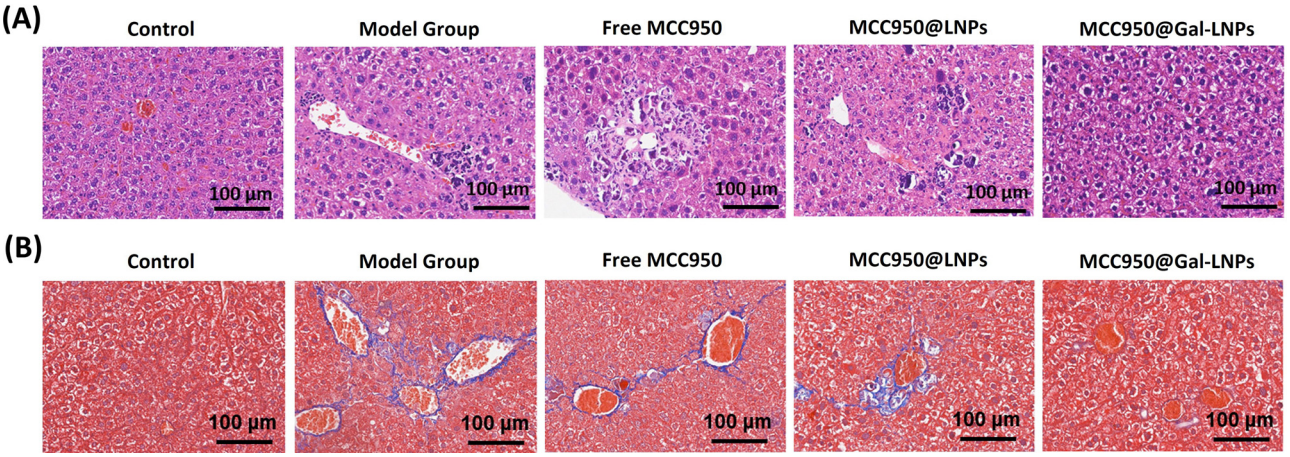


Fig. 7 Pathological analysis of liver tissue from MASLD mice after treatment. (A) Representative H&E staining images and (B) Masson staining images of mouse liver slices in different treatment groups.

BALB/c mice (random gender) in 6–8 weeks were purchased from Shanghai Model Organisms Center, Inc. (Shanghai, China). All animal experiments were approved by the Institutional Animal Care and Use Committee (IACUC) of the Animal Experiment Center of Nanjing Lishui People's Hospital (No. 20240511-0024). All mice were housed in an SPF-grade pathogen-free environment.

### MCC950@Gal-LNPs formulation and characterization

MCC950@LNPs and MCC950@Gal-LNPs were prepared by nanoprecipitation assay. Prescribed amounts of MCC950, DOPE, DODAP, cholesterol, and DSPE-PEG2000/DSPE-PEG2000-Gal were dissolved in methanol as an organic phase. Then, the organic phase was added to the appropriate amount of buffer solution dropwise under vigorous magnetic stirring, and the mixture was stirred for at least 10 minutes. Rotary evaporation was used to remove the organic phase in the mixture, and MCC950-loaded formulations were collected and stored at 4 °C for further investigation.

### Formulation optimization

**Effect of buffer pH on LNP characterization.** The drug-loaded formulation was prepared as described before. The drug/total lipid ratio was fixed at 40% (w/w), and the lipid components were DODAP/cholesterol/DOPE/DSPE-PEG2000-Gal (50%/15%/25%/10%, w/w). To optimize the pH value of the aqueous buffer, we prepared HEPES buffer (10 mM) at pH values of 7.4, 6.8, 5.0, and 3.0, and the drug-loaded formulations were prepared in different HEPES buffers. After the formulation was prepared, the particle size, zeta potential, and PDI were measured as key parameters to evaluate the characteristics of the formulation.

**Effect of cholesterol content on LNP characterization.** The content of cholesterol in the MCC950@Gal-LNP formulation was also optimized. The drug/total lipid ratio was fixed at 40% (w/w), and the lipid components contain DODAP, cholesterol, DOPE, and DSPE-PEG2000-Gal. The mass ratio of DODAP:DOPE:DSPE-PEG2000-Gal was fixed at 5 : 2.5 : 1, and different amounts of cholesterol (5%, 15%, 25%, or 35% of the total lipid materials) were mixed with other lipids to prepare the LNPs with HEPES buffer (pH 7.4). After the formulation was prepared, the particle size, zeta potential, and PDI were measured as key parameters to evaluate the characteristics of the formulation.

**Effect of DSPE-PEG-Gal content on LNP characterization.** The content of DSPE-PEG/DSPE-PEG2000-Gal in the MCC950@Gal-LNP formulation was further optimized. The drug/total lipid ratio was fixed at 40% (w/w), and the lipid components contain DODAP, cholesterol, DOPE, and DSPE-PEG2000-Gal. The mass ratio of DODAP : DOPE : cholesterol was fixed at 5 : 2.5 : 1.5, and different amounts of DSPE-PEG2000-Gal (1%, 2.5%, 5%, or 10% of the total lipid material) were mixed with other lipids to prepare the LNPs with HEPES buffer (pH 7.4). After the formulation was prepared, the particle size, zeta potential, and PDI were measured as key parameters to evaluate the characteristics of the formulation.

**Effect of DSPE-PEG-Gal content on LNP characterization.** The content of DODAP in the MCC950@Gal-LNPs formulation was optimized. The drug/total lipid ratio was fixed at 40% (w/w), and the lipid components contain DODAP, cholesterol, DOPE, and DSPE-PEG2000-Gal. The mass ratio of DOPE : cholesterol : DSPE-PEG2000-Gal was fixed at 5 : 3 : 2, and different amounts of DODAP (20%, 30%, 40%, or 50% of total lipid material) were mixed with other lipids to prepare the LNPs with HEPES buffer (pH 7.4). After the formulation was prepared, the particle size, zeta potential, and PDI were measured as key parameters to evaluate the characteristics of the formulation.

**Effect of the drug/lipid ratio on LNP characterization.** At last, the drug/total lipid ratio in MCC950@Gal-LNPs formulation was optimized. The components of DODAP/cholesterol/DOPE/DSPE-PEG2000-Gal were fixed with a certain ratio (50%/15%/25%/10%, w/w), respectively. The drug/total lipid ratio was adjusted from 5% to 40%. The LNPs were then prepared with HEPES buffer (pH 7.4). After the formulation was prepared, the particle size, zeta potential, and PDI were measured as key parameters to evaluate the characteristics of the formulation.

### Stability of MCC950@Gal-LNPs

Based on the formulation optimization, the MCC950@Gal-LNPs and MCC950@LNPs were successfully prepared, and their stability was further evaluated. The MCC950@LNPs and MCC950@Gal-LNPs were stored at 37 °C, respectively, and the particle size and PDI of LNPs were measured at different time intervals (2 h, 4 h, 6 h, 12 h, and 24 h).

### MCC950@Gal-LNPs inhibited inflammation in MASLD cell model

**MASLD cell model.** Normal AML-12 cells were used for MASLD cell model establishment by co-culture with free fatty acid molding fluid. The free fatty acid molding fluid was prepared based on the literature report. 30.5 mg of oleic acid and 13.9 mg of palmitic acid were precisely weighed and dissolved in 1 mL of PBS at 70 °C to prepare solution A. Solution A was diluted 10 times to obtain the free fatty acid molding fluid, which contains 10 mM of oleic acid and 5 mM of palmitic acid. The free fatty acid molding fluid was filtered by a 0.22 μm microporous filter membrane three times. The AML-12 cells were seeded in a 6-well plate and co-culture with free fatty acid molding fluid at high concentration (final concentration with 1 mM oleic acid and 0.5 mM palmitic acid) and low concentration (final concentration with 0.5 mM oleic acid and 0.25 mM palmitic acid), respectively. After 24 h incubation, the cells were washed with PBS three times, fixed by 4% paraformaldehyde fix solution, and stained with Oil Red O for 15 min. After washed by PBS, the cells were analyzed using an inverted microscope (Nikon, ECLIPSE Ts2R) to confirm the intracellular lipid accumulation.

### MCC950@Gal-LNPs inhibited inflammatory cytokines in the MASLD cell model

MASLD cell inflammation was induced by co-incubation with LPS for 24 h at a concentration of 10 ng $mL^{-1}$. To evaluate the MASLD treatment or MASLD prevention ability, inflammatory MASLD cells were co-incubated with various MCC950-loaded formulations for six hours, respectively. To evaluate the effects of MCC950 in MASLD treatment and prevent it, we regulated the cell incubation order of MCC950 and LPS. The activation of NF-κB based inflammation was determined by the qPCR assay and western blot assay.

For the qPCR assay, cells treated with various MCC950-loaded formulations were washed and lysed, and total RNA was extracted using RNAeasy™ RNA Isolation Kit. A multiscribe reverse transcription kit was employed to convert total RNA to cDNA per the manufacturer's instruction (Applied Biosystems). Taq Pro Universal SYBR qPCR Master Mix kit was used to run RT-PCR on a LightCycler 480 Instrument (Roche) using primers (NF-κB/p65 forward primer 5′-ATCTGCCGAGTGAACCGAAACT-3′, reverse primer 5′-CCAGCCTGG TCCCGTGAAA-3′; TNF-α forward primer 5′-CCTGTGAGGAGGACGAAC-3′, reverse primer 5′-CCTGTGAGGAGGACGAAC-3′; β-actin forward primer 5′-CAC GATGGAGGGGCCGGACTCATC-3′, reverse primer 5′-TAAAGAC CTCTATGCCAACACAGT-3′).

For the western blot assay, cells treated with various MCC950-loaded formulations were washed with PBS and lysed with RIPA buffer, followed by centrifugation at 12 000 rpm for 10 min at 4 °C. The total protein was collected and protein concentration was determined by the BCA kit. Total protein was mixed with loading buffer and denatured by the boiling process. The proteins were separated by SDS-PAGE, transferred to a PVDF membrane, and incubated with NF-κB and TNF-α primary antibodies at 4 °C overnight. The membrane was then washed with TBST and incubated with secondary antibodies at room temperature for one hour. The binds of the targeted proteins were imaged using a gel image system (Tanon 2500/2500R, Tanon, CN). The grey density of bands was further analyzed using the ImageJ software.

### Biodistribution

**MASLD mouse model.** MASLD mouse models were established by carbon tetrachloride ($CCl_4$) induction combined with a high-fat diet (HFD). The BALB/c mice were fed the high-fat diet for four weeks and injected with $CCl_4$ olive oil solution (20%, w/w) intraperitoneally every two days for four weeks, starting from the third week (0.1 mL per mouse). For the control group, mice were only fed a standard diet without $CCl_4$ olive oil solution induction.

**Biodistribution of MCC950@Gal-LNPs.** The biodistribution of MCC950-loaded formulation was investigated using the MASLD model mice. MASLD model mice were separated into three groups randomly: free DiD group, DiD@LNPs group, and DiD@Gal-LNPs group ($n$ = 3). For different groups, free DiD, DiD@LNPs group, and DiD@Gal-LNPs were administered intravenously in mice at the same dose (2 mg $kg^{-1}$ of DiD), respectively. After injection, the DiD signals were monitored at different time intervals (1 h, 4 h, 8 h, 24 h, and 48 h) using the IVIS instrument. Mice in each group were euthanized after a 48 h time interval, and major organs and serum were collected for IVIS imaging.

### MCC950@Gal-LNPs regulate MASLD *in vivo*

MASLD mice were randomly separated into four groups: MASLD model group, free MCC950 group, MCC950@LNPs group, and MCC950@Gal-LNPs group. Mice in different groups were treated with PBS or various MCC950 formulations (2 mg $kg^{-1}$) every three days for a total of five times, respectively. Mouse body weight was monitored during the treatment. On day fourteen, mice were euthanized using carbon dioxide inhalation at a flow rate of 10 L $min^{-1}$ for 10 min. Then, we monitored mice for five minutes for the following signs to confirm death: no rising and falling of chest, no palpable heartbeat, no response to toe pinch, and color change in eyes. Then, major organs and serum were collected.

The liver in different groups was separated into two parts for investigation. Half of the liver tissue was homogenized, and cells were lysed. Total protein was collected, and expression of α-SMA and TGF-β at the protein level was analyzed using the western blot assay. Total RNA in liver tissue was also extracted using the Trizol reagent, and mRNA levels of IL-6 and NLRP3

 

were determined using the qPCR assay (IL-6 forward primer 5′-GTTCTCTGGGAAATCGTGGA-3′, reverse primer 5′-TGTACTCCAGGTAGCTATGG-3′; NLRP3 forward primer 5′-TCACAACTCGCCCAAGGAGGAA-3′, reverse primer 5′-AAGAGACCACGGCAGAAGCTAG-3′; GAPDH forward primer 5′-CCTGCTTCACCACCTTCTTG-3′, reverse primer 5′-TGTCCGTCGTGGATCTGAC-3′;). The liver damage situation was monitored by measuring ALT and AST levels in the collected serum, which followed the instructions from the manufacturer. The other half of the liver and other major organs were fixed, embedded, and further stained with hematoxylin–eosin (H&E) and Masson reagent. All tissue sections were scanned, and representative views of sections are shown.

### Statistical analysis

All experiments were conducted in triplicate. Statistical differences between means were determined by SPSS using the One-way ANOVA where $p < 0.05$ was considered statistically significant. All values are reported as mean ± SD.

## Conclusions

In summary, we designed a galactose-modified lipid nanoparticle system for MCC950 liver-targeted delivery. Drug-loaded vesicles (MCC950@Gal-LNPs) could effectively deliver the MCC950 target and extend accumulation in the liver. The MCC950 could reduce inflammatory-related signaling pathway activation and attenuate inflammation-induced liver fibrosis in the MASLD mouse model, suggesting that MCC950 is a potential liver fibrosis therapeutic agent worthy of further preclinical investigation.

## Author contributions

Chunyan Niu: writing – original draft, supervision, project administration, methodology, funding acquisition, and conceptualization. Jinming Yang: supervision, funding acquisition, and conceptualization. Wen Gao: writing – original draft, project administration, and methodology. Mei Tan: writing – original draft, project administration, and methodology. Yue Chen: formal analysis and data curation. Yongqiang Shi: formal analysis and data curation. Yan Geng: software and formal analysis. Tingting Zhang: software and formal analysis. Huayi Tao: software and formal analysis. Zhenjiang Xu: software and formal analysis. All authors discussed the results and commented on the manuscript. Dr. Chunyan Niu working as responsible corresponding author.

## Conflicts of interest

There are no conflicts to declare.

## Data availability

The data supporting this article have been included as part of the supplementary information (SI). Supplementary information is available. See DOI: https://doi.org/10.1039/d5tb02289d.

## Acknowledgements

Dr. Chunyan Niu working as responsible corresponding author. This work was supported by the Nanjing Medical Science and Technology Development Fund (No. YKK22240), the 2024 Lishui People's Hospital Medical and Health High Quality Development Science and Technology Special Fund Project Plan (No. LWG202405), and The Initial Scientific Research Fund of the Talents Introduced in Nanjing Lishui People's Hospital (No. 2021YJ02).

## Notes and references

1 K. Pafili and M. Roden, *Mol. Metab.*, 2021, **50**, 101122.
2 E. Buzzetti, M. Pinzani and E. A. Tsochatzis, *Metabolism*, 2016, **65**, 1038–1048.
3 F. Shirazi, J. Wang and R. J. Wong, *J. Clin. Exp. Hepatol.*, 2020, **10**, 30–36.
4 X. Wang, L. Zhang and B. Dong, *Hepatology*, 2025, **82**, 1303–1324.
5 R. F. Schwabe, I. Tabas and U. B. Pajvani, *Gastroenterology*, 2020, **158**, 1913–1928.
6 Q. M. Anstee, H. L. Reeves, E. Kotsiliti, O. Govaere and M. Heikenwalder, *Nat. Rev. Gastroenterol. Hepatol.*, 2019, **16**, 411–428.
7 X. Xu, K. L. Poulsen, L. Wu, S. Liu, T. Miyata, Q. Song, Q. Wei, C. Zhao, C. Lin and J. Yang, *Signal Transduction Targeted Ther.*, 2022, **7**, 287.
8 J. Ma, M. Li, T. Yang, Y. Deng, Y. Ding, T. Guo and J. Shang, *Int. J. Mol. Sci.*, 2023, **24**, 8795.
9 H. Tilg, A. R. Moschen and M. Roden, *Nat. Rev. Gastroenterol. Hepatol.*, 2017, **14**, 32–42.
10 M. Eslam, A. J. Sanyal, J. George and I. C. Panel, *Gastroenterology*, 2020, **158**(1999–2014), e1991.
11 H. Nakagawa, *World J. Hepatol.*, 2015, **7**, 2110–2118.
12 R. Kumar, B. G. Goh, J. W. Kam, P. E. Chang and C. K. Tan, *Clin. Mol. Hepatol.*, 2020, **26**, 196–208.
13 P. Horn and P. N. Newsome, *Expert Opin. Ther. Targets*, 2020, **24**, 175–186.
14 C. L. Chen and Y. C. Lin, *Int. J. Mol. Sci.*, 2022, **23**, 10055.
15 Z. Weng, C. Xu, X. Zhang, L. Pang, J. Xu, Q. Liu, L. Zhang, S. Xu and A. Gu, *Environ. Pollut.*, 2020, **267**, 115655.
16 F. Marín-Aguilar, B. Castejón-Vega, E. Alcocer-Gómez, D. Lendines-Cordero, M. A. Cooper, P. de la Cruz, E. Andújar-Pulido, M. Pérez-Alegre, J. Muntané, A. J. Pérez-Pulido, B. Ryffel, A. A. B. Robertson, J. Ruiz-Cabello, P. Bullón and M. D. Cordero, *J. Gerontol., Ser. A*, 2020, **75**, 1457–1464.
17 I. C. Yen, J. C. Lin, Y. Chen, Q. W. Tu and S. Y. Lee, *Am. J. Chin. Med.*, 2020, **48**, 1859–1874.
18 W. Yuan, T. Qiu, X. Yao, C. Wu, Y. Shi, N. Wang, J. Zhang, L. Jiang, X. Liu, G. Yang, J. Bai and X. Sun, *Toxicol. Lett.*, 2022, **370**, 7–14.
19 A. Wree, T. M. Holtmann, M. E. Inzaugarat and A. E. Feldstein, *Semin. Liver Dis.*, 2019, **39**, 275–282.
20 Y. F. Deng, Q. Q. Xu, T. Q. Chen, J. X. Ming, Y. F. Wang, L. N. Mao, J. J. Zhou, W. G. Sun, Q. Zhou, H. Ren and Y. H. Zhang, *Phytomedicine*, 2022, **104**, 154241.

21 A. R. Mridha, A. Wree, A. A. B. Robertson, M. M. Yeh, C. D. Johnson, D. M. Van Rooyen, F. Haczeyni, N. C. Teoh, C. Savard, G. N. Ioannou, S. L. Masters, K. Schroder, M. A. Cooper, A. E. Feldstein and G. C. Farrell, *J. Hepatol.*, 2017, **66**, 1037–1046.
22 H. Li, Y. Guan, B. Liang, P. Ding, X. Hou, W. Wei and Y. Ma, *Eur. J. Pharmacol.*, 2022, **928**, 175091.
23 R. Ward, W. Li, Y. Abdul, L. Jackson, G. Dong, S. Jamil, J. Filosa, S. C. Fagan and A. Ergul, *Pharmacol. Res.*, 2019, **142**, 237–250.
24 S. Ghosh, C.-J. Yang and J.-Y. Lai, *Prog. Mater. Sci.*, 2026, **158**, 101634.
25 S. Ghosh, C. J. Yang and J. Y. Lai, *Mater. Today Bio*, 2025, **35**, 102442.
26 D. D. Nguyen and J.-Y. Lai, *Chem. Eng. J.*, 2022, **435**, 134970.

 